



POTSDAM-INSTITUT FÜR
KLIMAFOLGENFORSCHUNG

Originally published as:

Boisier, J. P., de Noblet-Ducoudré, N., Pitman, A. J., Cruz, F. T., Delire, C., van den Hurk, B. J. J. M., van der Molen, M. K., Müller, C., Voldoire, A. (2012): Attributing the impacts of land-cover changes in temperate regions on surface temperature and heat fluxes to specific causes: Results from the first LUCID set of simulations. - Journal of Geophysical Research, 117, D12116

DOI: [10.1029/2011JD017106](https://doi.org/10.1029/2011JD017106)

Available at <http://onlinelibrary.wiley.com>

© American Geophysical Union

Attributing the impacts of land-cover changes in temperate regions on surface temperature and heat fluxes to specific causes: Results from the first LUCID set of simulations

J. P. Boisier,¹ N. de Noblet-Ducoudré,¹ A. J. Pitman,² F. T. Cruz,^{3,4} C. Delire,⁵ B. J. J. M. van den Hurk,⁶ M. K. van der Molen,^{6,7} C. Müller,⁸ and A. Voldoire⁵

Received 9 November 2011; revised 28 March 2012; accepted 21 May 2012; published 30 June 2012.

[1] Surface cooling in temperate regions is a common biogeophysical response to historical Land-Use induced Land Cover Change (LULCC). The climate models involved in LUCID show, however, significant differences in the magnitude and the seasonal partitioning of the temperature change. The LULCC-induced cooling is directed by decreases in absorbed solar radiation, but its amplitude is 30 to 50% smaller than the one that would be expected from the sole radiative changes. This results from direct impacts on the total turbulent energy flux (related to changes in land-cover properties other than albedo, such as evapotranspiration efficiency or surface roughness) that decreases at all seasons, and thereby induces a relative warming in all models. The magnitude of those processes varies significantly from model to model, resulting on different climate responses to LULCC. To address this uncertainty, we analyzed the LULCC impacts on surface albedo, latent heat and total turbulent energy flux, using a multivariate statistical analysis to mimic the models' responses. The differences are explained by two major 'features' varying from one model to another: the land-cover distribution and the simulated sensitivity to LULCC. The latter explains more than half of the inter-model spread and resides in how the land-surface functioning is parameterized, in particular regarding the evapotranspiration partitioning within the different land-cover types, as well as the role of leaf area index in the flux calculations. This uncertainty has to be narrowed through a more rigorous evaluation of our land-surface models.

Citation: Boisier, J. P., N. de Noblet-Ducoudré, A. J. Pitman, F. T. Cruz, C. Delire, B. J. J. M. van den Hurk, M. K. van der Molen, C. Müller, and A. Voldoire (2012), Attributing the impacts of land-cover changes in temperate regions on surface temperature and heat fluxes to specific causes: Results from the first LUCID set of simulations, *J. Geophys. Res.*, 117, D12116, doi:10.1029/2011JD017106.

1. Introduction

[2] Land-cover conversion has increased significantly over the last 300 years and, nowadays, more than half of the

global land surface is perturbed by humans to some degree [Ellis *et al.*, 2010]. Since the preindustrial epoch, croplands and rangelands have expanded, mainly through the removal of natural forest and grasslands in the temperate regions of the Northern Hemisphere [Ramankutty and Foley, 1999; Hurtt *et al.*, 2006; Ellis *et al.*, 2010; Klein Goldewijk *et al.*, 2011].

[3] Land-Use induced Land-Cover Changes (LULCC) affect climate through many ways, some being changes in the continental energy and water surface budgets. Such biogeophysical impacts of LULCC have received special attention in the last two decades (e.g., Betts *et al.* [2007] and Pitman *et al.* [2009] at global scale and Pielke *et al.* [2011, and references therein] at regional scale), but still remain uncertain as they depend on many factors, such as for example the scale of perturbation and its geographical location (e.g., tropics, temperate or boreal lands).

[4] Studies using global climate models (GCMs) generally agree that historical LULCC has increased the surface albedo in regions where forests have been cleared, many of them showing this effect and the associated near surface

¹Laboratoire des Sciences du Climat et de l'Environnement, Unité Mixte CEA-CNRS-UVSQ, Gif-sur-Yvette, France.

²ARC Centre of Excellence for Climate System Science, University of New South Wales, Sydney, New South Wales, Australia.

³Climate Change Research Centre, University of New South Wales, Sydney, New South Wales, Australia.

⁴Manila Observatory, Quezon City, Philippines.

⁵Groupe d'Étude de l'Atmosphère Météorologique, Unité Associée CNRS/Météo-France, Toulouse, France.

⁶Royal Netherlands Meteorological Institute, De Bilt, Netherlands.

⁷Meteorology and Air Quality Group, Wageningen University and Research Centre, Wageningen, Netherlands.

⁸Earth System Analysis, Potsdam Institute for Climate Impact Research, Potsdam, Germany.

Corresponding author: J. P. Boisier, Laboratoire des Sciences du Climat et de l'Environnement, Unité Mixte CEA-CNRS-UVSQ, Bat.712, Orme des Merisiers, Point Courrier 132, FR-91191 Gif-sur-Yvette CEDEX, France. (juan-pablo.boisier@lscce.ipsl.fr)

cooling as the leading impact of LULCC [Hansen et al., 1998; Govindasamy et al., 2001; Feddema et al., 2005b]. The global negative radiative forcing induced by surface albedo increases has therefore been estimated in several studies [Betts, 2001; Matthews et al., 2003; Myhre and Myhre, 2003; Betts et al., 2007; Davin et al., 2007; among others] and has been commonly used to measure the historical impact of LULCC [Forster et al., 2007]. However, a number of authors have alerted the community that non-radiative processes (i.e. alteration of surface fluxes) can also have large impacts on surface and air temperature, or precipitation [e.g., National Research Council, 2005; Davin et al., 2007].

[5] The radiatively induced cooling at the surface may be enhanced or reduced by non-radiative processes including the partitioning of net radiation between latent and sensible heat [Bonan, 2008]. Temperate forest clearing may lead to evaporative cooling during spring and summer time because crops often have larger evaporation rates than forests if the water supply is sufficient [Baldocchi et al., 1997; Oleson et al., 2004; Mahmood et al., 2006; Puma and Cook, 2010; Teuling et al., 2010]. In contrast, strong decreases in latent heat flux resulting in net warming have been found at lower latitudes because the cropping systems in those regions are not as productive and efficient as in the developed temperate regions [Bounoua et al., 2002; Snyder et al., 2004; Lawrence and Chase, 2010], which echo the future projections of the LULCC-induced impacts in the tropics [Feddema et al., 2005a]. While the two mechanisms mentioned above have a direct impact on the latent/sensible heat flux partitioning, LULCC in the form of deforestation could also reduce the magnitude of the ensemble of turbulent energy fluxes increasing surface temperatures through changes in surface roughness [Davin and de Noblet-Ducoudré, 2010].

[6] At smaller spatial scales (local to regional), there have been a number of observations [e.g., Loarie et al., 2011; Butt et al., 2011; Lyons et al., 1993, 2008] and numerical simulations [e.g., Marshall et al., 2004; Gero et al., 2006; Georgescu et al., 2011] that have highlighted the complexity of land-atmosphere interactions, the multiple ways through which LULCC may impact the atmospheric and surface states, the land-atmosphere exchanges and therefore the atmospheric circulation at those scales, as reported in more details in Pielke et al. [2011].

[7] Besides all these studies and some consistent regional climate signals, the net and robust effect of the different land-surface processes relevant to LULCC and the resulting impacts on surface temperatures and precipitation remain unclear at the large scale. Significant differences in land-use/land-cover representation and in the simulated biophysical processes are behind the uncertainties found by various modeling studies [Matthews et al., 2003; Myhre and Myhre, 2003; Oleson et al., 2004; Feddema et al., 2005b; Forster et al., 2007; de Noblet-Ducoudré et al., 2012].

[8] Within the framework of the international IGBP/iLEAPS and GEWEX/GLASS project ‘Land-Use and Climate, Identification of robust impacts’ (LUCID), an experimental design was conceived to assess the robust global biogeophysical impacts of LULCC on climate from the preindustrial period to present-day, using several GCMs forced with the same land-use datasets and using the same modeling protocol. Pitman et al. [2009] described the first

results of LUCID at the global-scale for the Northern Hemisphere summer. They showed statistically significant impacts of LULCC on the simulated near-surface temperature and latent heat flux over the regions where the LULCC were imposed. Most models simulate cooling, but the strength of the changes varies considerably. The latent heat flux responses are even more heterogeneous, with different signs and amplitudes. de Noblet-Ducoudré et al. [2012] further explored those results and the reasons behind the variety of LULCC-induced responses in North America and Eurasia. One important finding of their analysis is that, although the dispersion among the models’ response to LULCC is large, there are a number of robust common features shared by all models. Absence of consistency only regards how LULCC affects the partitioning of available energy between latent and sensible heat fluxes at a specific time in the various models. Quite importantly as well, they showed that, regionally, LULCC has an impact on the near surface temperatures and other variables of similar magnitude (opposite in sign) than the resulting from increased greenhouse gases and a warmer ocean that occurred during the same time period. This in itself reinforces the message brought forward by scientists working at the regional level, arguing that LULCC has the potential to significantly affect climate and should be accounted for in detection/attribution studies and projections of climate change at smaller scales.

[9] This paper builds on de Noblet-Ducoudré et al. [2012] to a) examine the mechanisms through which the models involved in LUCID respond to LULCC, and b) try to explain why some of their responses to LULCC diverge. We quantify the causes of the inter-model dispersion focusing on the relative role of two key components. First, variations in the land-cover distribution that may largely differ from one model to another. Second, the individual GCM’s sensitivity to the imposed LULCC, which includes how land-surface processes are parameterized and how these represent, and respond to, a land-cover perturbation.

[10] Our analyses focus on changes in the surface energy balance and particularly on the boreal summer (JJA) and winter (DJF) changes of surface albedo, latent heat flux and total turbulent energy flux, since these are the key variables that explain the radiative and non-radiative impacts of LULCC. We used statistical models of these variables to estimate the responses of each GCM to a limited number of drivers, notably, to perturbations in the land cover partitioning. We used the statistically based models as benchmark to assess the various LUCID GCMs in a similar approach of that of Koster and Milly [1997] and Abramowitz [2005]. The LUCID experimental design and used methodology are presented in section 2. Section 3 describes the LULCC impacts on the different components of the surface energy budget and the resulting temperature changes. The attribution of the LULCC-induced changes on surface climate and a diagnosis of the inter-model dispersion are presented in section 4. Conclusions are provided in section 5.

2. Material and Methods

2.1. LUCID Simulations

[11] The LUCID simulations analyzed here are the same as those described in Pitman et al. [2009] and de Noblet-Ducoudré et al. [2012] (hereafter N2012). Four types of

Table 1. Simulations Carried out Within the LUCID Intercomparison Project^a

Experiment Name	Land-Cover Year	SST/SIC Period	CO ₂ (ppm)
PD	1992	1970–1999	375
PDv	1870	1970–1999	375
PI	1870	1870–1899	280
PIv	1992	1870–1899	280

^aPrescribed land-cover maps years, sea-surface temperature/sea-ice concentrations (SST/SIC) period and atmospheric CO₂ concentrations.

simulations were conducted by seven global climate models (GCMs) to evaluate the impact of LULCC from the preindustrial period to present day. Each experiment includes an ensemble of 30-years simulations (five members), computed with prescribed sea surface temperatures (SSTs) and sea-ice concentration (SIC), atmospheric CO₂ concentrations ([CO₂]) and land-cover maps (Table 1). All the models used the same SST/SIC HadISST dataset of Rayner *et al.* [2003] and a combined crop/pasture data set of Ramankutty and Foley [1999] and Klein Goldewijk [2001]. The preindustrial (PI) and present-day (PD) experiments used the prescribed data of the corresponding period, with interannual variability being accounted for uniquely for SSTs and SIC. Another experiment (PDv) was also performed using the present-day SST, SIC and [CO₂] (hereafter SST/CO₂) and the preindustrial vegetation (set to 1870). Finally, experiment PIV used the preindustrial SST/CO₂ with the current vegetation (1992). Thus, the isolated effect of LULCC between 1870 and 1992 is defined by both differences PD – PDv and PIV – PI. All simulations have been run in an ensemble mode to include more robustness in the results reported herein.

[12] In this study we explore the main effect of land-use embedded in both SST/CO₂-related climate states, and will refer to the LULCC-induced anomaly of a generic variable Y as

$$\Delta Y = \frac{1}{2}(Y_{PD} - Y_{PDv} + Y_{PIv} - Y_{PI}) \quad (1)$$

where Y_E is the climatological value of Y in a given experiment E .

[13] The seven GCMs involved in LUCID and the land surface models (LSMs) embedded in each GCM (hereafter GCM/LSMs), are ARPEGE/ISBA [Salas-Méla *et al.*, 2005; Voldoire, 2006], CCAM/CABLE [McGregor and Dix, 2008; Abramowitz *et al.*, 2008], CCSM/CLM [Collins *et al.*, 2006; Oleson *et al.*, 2008], ECEARTH/TESSSEL [van den Hurk *et al.*, 2000], ECHAM5/JSBACH [Roeckner *et al.*, 2006; Raddatz *et al.*, 2007], IPSL/ORCHIDEE [Marti *et al.*, 2010; Krinner *et al.*, 2005] and SPEEDY/LPJmL [Strengers *et al.*, 2010; Bondeau *et al.*, 2007]. For further details on the experiment setup and model descriptions, see N2012.

2.2. Methodology

[14] Results from the LUCID simulations show clear impacts on the near-surface temperature and latent heat flux in regions where the land-cover is perturbed, and do not show statistically significant signals elsewhere [Pitman *et al.*, 2009]. Therefore, we focus our analysis on areas where the imposed LULCC is significant. Two regions in respectively North America and west Eurasia were defined where the absolute change in the fraction of the surface occupied by crops or pastures between 1870 and 1992 exceeds 5% (Figure 1). In this study we do not show specific comparison between these two regions (while N2012 did), so the analyses are related to the combined overall North American and Eurasian region (hereafter NAEA). We focus on the temperate mid-latitudes because Pitman *et al.* [2009] and N2012 showed these regions to be particularly sensitive to historical LULCC.

[15] Our analysis is based on the components of the surface energy budget (SEB):

$$Q_{SN} + Q_{LD} = Q_T + Q_{LU} + Q_R \quad (2)$$

$$Q_{SN} = (1 - \alpha)Q_{SD} \quad (3)$$

where Q_{SN} and Q_{SD} are the net and downward shortwave radiation, Q_{LD} and Q_{LU} the downward and upward longwave radiation, Q_T the sum of the latent (Q_{LE}) and sensible (Q_H) heat fluxes, Q_R a residual term (all values are in Wm⁻²), and α is the surface albedo. In order to have a closed SEB

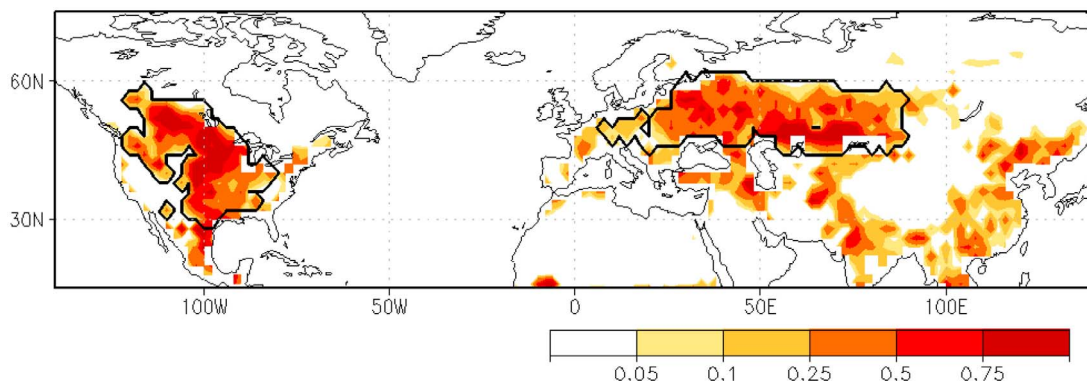


Figure 1. Absolute changes in crop and pasture fractions between 1870 and 1992. Solid contours indicate areas with changes larger than 5% in crop or pasture fractions confined to North America and west Eurasia (NAEA).

Table 2. Regressed (Predictands) and Explanatory (Predictors) Variables Used in Multivariate Statistical Analyses^a

Predictand	Predictor
α	F_v, LAI, SWE
Q_{LE}, Q_T	F_v, LAI, Q_{SN}, R, R_-

^a α : Surface albedo. Q_{LE} : Latent heat flux. Q_T : Total turbulent energy flux. F_v : Land-cover fractions [evergreen trees (F_v), deciduous trees (F_d), crops (F_c), grasses (F_g), bare soil (F_s)]. LAI : Leaf area index. SWE : Snow water equivalent. Q_{SN} : Net shortwave radiation. R : Precipitation. R_- : 1-season lag precipitation.

relation, Q_R is derived explicitly from the other terms in equation (2), and accounts for the energy fluxes not considered here (the soil heat flux principally).

[16] The results described in section 4 are based on multivariate statistical analyses. Linear regressions of α , Q_{LE} and Q_T were computed for each GCM/LSM within the NAEA region from a set of predictors including surface and atmospheric variables. In order to account for the land-surface properties related to the different types of vegetation, the grid-fractions occupied by the various land-cover types were used as part of these predictors in all analyses. In most of the LSMs assessed here, the biogeography is represented through Plant Functional Types (PFTs). Depending on the model, the grid cell includes one (CABLE), two (TESSEL) or multiple PFTs (CLM, JSBACH, ORCHIDEE, LPJmL). In the case of ISBA, a set of parameters, averaged from those of the different PFTs co-existing within each grid-cell, describes the vegetation-related grid properties. Considering this, the regression models for the three analyzed variables were based on a mosaic approach of the sub-grid heterogeneity; that is, the grid mean value of a generic land-surface quantity Y_g is obtained as the linear combination of the components associated with the different land cover types present in the grid-cell, i.e.,

$$Y_g = \sum_v F_v Y_v \quad (4)$$

where F_v is the grid area fraction of the land-cover type v and Y_v is the associated tile value of Y .

[17] To have consistent land-cover types across the models, the various PFTs used in the different LSMs were grouped in four main vegetation classes (evergreen trees, deciduous trees, grasses and crops), in addition to bare soil. These five land-cover types were then used in the regression analysis.

[18] Our objective here is to evaluate the sensitivity of each GCM/LSM to the same historical LULCC perturbation or change in another predictor. Our method therefore estimates seasonal anomalies rather than absolute values. This choice also helps to minimize the effect of non-linear relationships (e.g., soil water availability versus evapotranspiration), and avoid the spatial variability of some surface properties that do not change between the various experiments and that are not assessed here (e.g., soil color). For each GCM/LSM, the seasonal anomalies (Y'_g) represent departures from the climatological mean state of all four experiments ($\overline{Y_g}$). The statistical models we used take the first order terms of the

expansion of equation (4) when applying perturbed forms of Y_g , Y_v and F_v . The functions regressed have then the form:

$$Y'_g(\mathbf{P}) = \sum_v [F'_v \overline{Y}_v(\mathbf{P}) + \overline{F}_v Y'_v(\mathbf{P})]. \quad (5)$$

[19] The first term on the right-hand side of equation (5) represents the direct effect of LULCC led by changes in the land-cover partitioning (F'_v) and accounts for grid-mean change in the surface properties resulting from the vegetation perturbation. The second term represents the indirect impact led by a perturbation in the tile values of Y'_g (Y'_v), which is driven by changes in the environmental variables (e.g., the contribution of snow-cover change to the surface albedo response).

[20] The array \mathbf{P} represents the set of predictors used (Table 2) excluding the land-cover fractions F_v , which are explicitly taken in account in equation (5). The seasonal mean state \overline{Y}_v and the corresponding anomaly Y'_v are modeled as polynomial expansions over the components of \mathbf{P} (see Appendix A).

[21] For the Q_{LE} and Q_T analysis, the explanatory variables included in \mathbf{P} were the seasonal means of leaf area index (LAI), net shortwave radiation (Q_{SN}) and precipitation (R), in addition of a 1-season lag precipitation value (R_-). The latter was included to take into account the effect of soil moisture memory [Seneviratne et al., 2006]. The surface energy supply by radiation was considered using only Q_{SN} . Longwave radiation fluxes are explicitly isolated because they have the potential to mislead the interpretation of the regression results, as they are highly coupled with other drivers and predictands.

[22] The surface roughness (Z_0) is another important driver of Q_{LE} and Q_T , but it was not considered here because it is highly correlated with the forest fraction (Table 3) and, therefore, implicitly accounted for through F_v . On the same ground, depending on the model, the role that LAI plays in the three assessed predictands should be interpreted with caution, since it may also be significantly collinear with the forest fraction (Table 3). The results shown in section 4.2 were obtained from a second analysis carried out without using LAI as a predictor. This simpler choice allows us to evaluate the statistical models with different land-cover forcings without losing consistency with the LAI patterns.

Table 3. Spatial Correlation Between Forest Fraction and Leaf Area Index ($r_{F,L}$), and Between Forest Fraction and Roughness Length ($r_{F,Z}$) in JJA

GCM/LSM	$r_{F,L}$	$r_{F,Z}$
ECEARTH/TESSEL	0.51	0.92
CCAM/CABLE	0.71	0.90
IPSL/ORCHIDEE	0.54	0.99
SPEEDY/LPJmL	0.65	0.92
ARPEGE/ISBA	0.71	0.93
ECHAM5/JSBACH	0.45	0.57
CCSM/CLM	0.88	0.88

Table 4. Winter (DJF) and Summer (JJA) LULCC-Induced Surface Temperature Changes (K) in NAEA^a

GCM/LSM	DJF		JJA	
	$\Delta_R T_S$	ΔT_S	$\Delta_R T_S$	ΔT_S
ECEARTH/TESSSEL	-1.62	-0.91	-1.33	-0.78
CCAM/CABLE	-0.14	-0.14	-0.32	-0.54
IPSL/ORCHIDEE	-0.81	-0.26	-0.41	0.43
SPEEDY/LPJmL	-0.99	-0.25	-0.39	-0.66
ARPEGE/ISBA	-1.11	-0.76	-0.81	-0.67
ECHAM5/JSBACH	-0.09	0.02	-0.29	-0.24
CCSM/CLM	-0.29	-0.11	-0.25	-0.19
MEAN	-0.72	-0.34	-0.54	-0.38

^a ΔT_S is the surface temperature changes simulated by each GCM/LSM, while $\Delta_R T_S$ are the ones expected from the sole changes in surface radiation. Values derived from changes in upward longwave radiation flux (following equations (6)–(8)).

[23] A more complete description of the statistical analysis, of the regression models used, and of the skills of the predicted responses, is provided in Appendix A.

3. How Strongly Do the Non-radiative Fluxes Contribute to the Temperature Changes?

[24] The simulated cooling in the NAEA region is a clear impact of LULCC on the surface climate in the ensemble of LUCID simulations, despite the inter-model spread (N2012). In both DJF and JJA the model-mean surface temperature anomalies (ΔT_S) averaged over NAEA are -0.34 K and -0.38 K respectively (Table 4). In DJF, the individual model responses range from -0.91 K (ECEARTH) to 0.02 K (ECHAM5). In JJA, the model spread is slightly greater, ranging from -0.78 K (ECEARTH) to $+0.43$ K (IPSL).

[25] Using equation (2) we can attribute the changes in surface temperature to changes in each of the SEB components. A perturbation in Q_{SN} , Q_{LD} , Q_T or Q_R can be expressed as an upward infrared radiation anomaly (ΔQ_{LU}),

by fixing the non-perturbed terms. Then, ΔT_S is calculated by inverting the Stefan-Boltzmann law:

$$\Delta T_S = (\epsilon\sigma)^{-1/4} \left[\left(Q_{LU}^* + \Delta Q_{LU}^* \right)^{1/4} - Q_{LU}^* / 4 \right] \quad (6)$$

where Q_{LU}^* is derived from the unperturbed components of SEB. The surface emissivity (ϵ) is set to 1.0.

[26] Figure 2 shows the monthly near-surface temperature change induced by LULCC in NAEA averaged over all the models (solid line). Dots and shaded bars indicate the net ΔT_S and the contributions from changes in the different SEB components (derived from equation (6)). Since the surface energy balance must be maintained, the simulated model-mean temperature response matches closely the one derived from the various SEB fluxes.

[27] The ensemble of LUCID models shows a cooling throughout the year dominated by a consistent decrease in available energy at the surface (defined here as the sum of the net shortwave and the downward longwave radiation; $Q_A = Q_{SN} + Q_{LD}$). The Q_A decreases are mainly driven by the albedo-induced reductions in net solar radiation (Q_{SN}) but also by reductions in the incoming long-wave radiation (Q_{LD}). Q_{LD} changes represent an indirect impact of LULCC and, in all models, are approximately proportional to the changes in T_S (not shown). This underlines the existence of a positive feedback between T_S and incident long-wave radiation as discussed by *van der Molen et al.* [2011] and reported in N2012. The Q_{SN} decrease is stronger during the early spring (March), when the model-mean T_S anomaly reaches about -0.5 K. The radiative impact is larger during this season due to a maximized effect of the forest-induced snow-masking albedo change combined with the increasing solar radiation availability.

[28] The component of ΔT_S induced by Q_R (white bars in Figure 2) is directed by changes in CCAM/CABLE and SPEEDY/LPJmL principally. The LULCC-induced Q_R changes are near zero in most models except for these two cases, which show quite large positive values. This highlights an

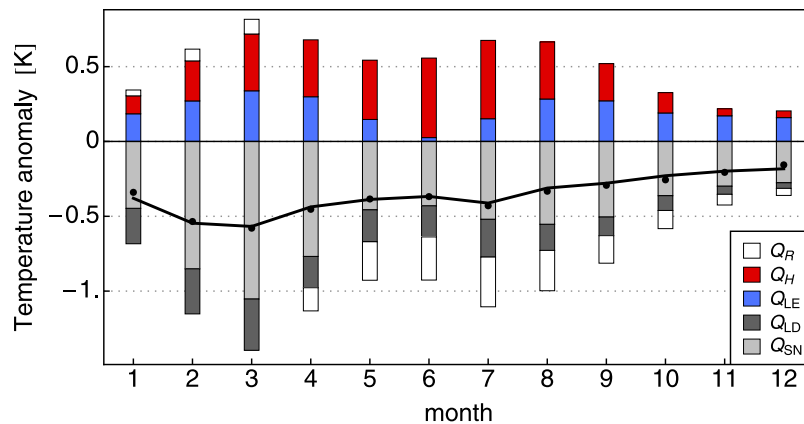


Figure 2. LULCC-induced monthly surface temperature anomalies derived from changes in the various components of the surface energy budget (inter-model average). Bars indicate the temperature anomaly induced by changes in latent heat flux (blue), in sensible heat flux (red), in net shortwave radiation (grey), in downward longwave radiation (dark grey) and in the residual term (white; see equation (2)). Dots indicate the computed net surface temperature anomalies (all components). Solid line indicates the model-mean of the simulated LULCC-induced monthly 2-m temperature anomalies.

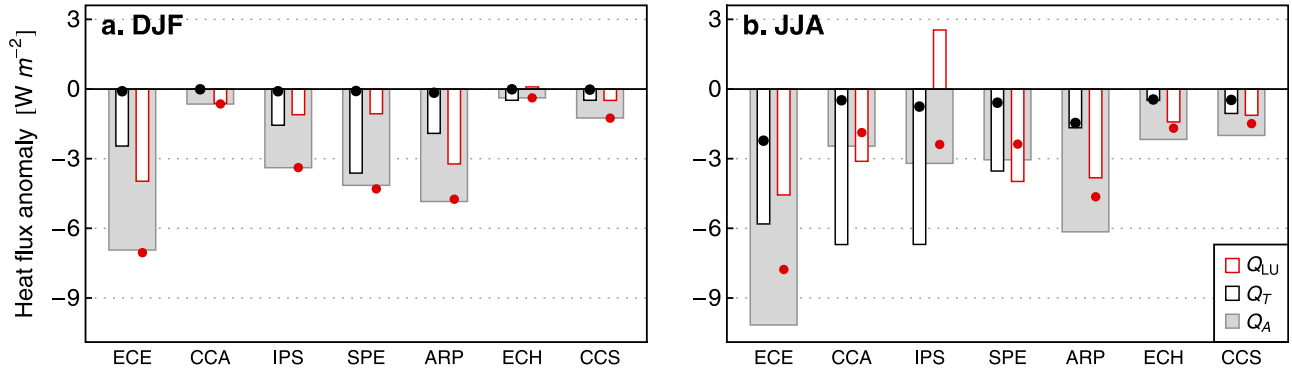


Figure 3. Seasonal LULCC-induced anomalies of available energy Q_A (gray bars), total turbulent energy flux Q_T (black edge bars) and upward longwave radiation Q_{LU} (red edge bars). Black and red dots indicate the anomalies of Q_T and Q_{LU} expected from the changes in Q_A (derived from equations (7) and (8)). ECE, CCA, IPS, SPE, ARP, ECH and CCS are the GCM/LSMs acronyms for respectively ECEARTH/ TESSEL, CCAM/CABLE, IPSL/ORCHIDEE, SPEEDY/LPJmL, ARPEGE/ISBA, ECHAM5/JSBACH and CCSM/CLM.

issue in the surface energy closure of CABLE and LPJmL, showing a lack of consistency between the surface temperature responses and the changes in the SEB components.

[29] In contrast to the impacts on radiative fluxes, the model-mean changes of sensible (Q_H) and latent (Q_{LE}) heat fluxes lead to a systematic warming (red and blue bars in Figure 2). The radiatively induced drop in T_S is therefore dampened by the warming effect due to the decrease in the ensemble of turbulent heat fluxes (Q_T). The Q_T anomalies are almost as large as those of Q_A during the summer (JJA) and, as shown below and discussed in N2012, they are much larger than one would expect from the surface radiation perturbations. Figure 3 highlights these changes in the breakdown of Q_A between Q_T and Q_{LU} during the winter (DJF) and summer (JJA), for each individual model in NAEA.

[30] When land-cover is set to its preindustrial conditions (i.e., the mean between the experiments *PI* and *PDv*; see Table 1) the partitioning of Q_A into Q_T and Q_{LU} , averaged over NAEA, is about 0.25 (Q_T/Q_A) and 0.75 (Q_{LU}/Q_A) in JJA, and 0.05 (Q_T/Q_A) and 0.95 (Q_{LU}/Q_A) in DJF (these ratios are quite similar from one model to another). If one assumes that those ratios do not change when land-cover changes, then the radiatively induced responses of Q_T and Q_{LU} can be estimated by:

$$\Delta_R Q_T = \left(\frac{Q_T}{Q_A} \right)_{pi} \Delta Q_A \quad (7)$$

$$\Delta_R Q_{LU} = \left(\frac{Q_{LU}}{Q_A} \right)_{pi} \Delta Q_A. \quad (8)$$

[31] These estimates, calculated for each model from equations (7) and (8), are shown in Figure 3 as black and red dots respectively. Most models show larger absolute changes in Q_T than expected by the perturbation to Q_A . Since the SEB must be maintained, these ‘extra’ (non radiatively induced) Q_T reductions are associated with weaker Q_{LU} responses (relative surface warming) than those expected from the Q_A anomaly. This effect is particularly strong in the IPSL/

ORCHIDEE case, model that therefore displays warming instead of cooling in JJA. Our conclusion does not hold for CCAM/CABLE and SPEEDY/LPJmL in JJA because their net changes (sum) of Q_T and Q_{LU} are larger than those of Q_A (i.e., large Q_R changes compared to the other models).

[32] Thus, the LULCC-induced reduction in Q_A plays a fundamental role explaining the surface cooling observed in most models and all seasons in NAEA. However, the large decrease in Q_T , which can partially be attributed to the LULCC-induced decrease in Z_0 , dampens this cooling. Quantitatively, the net effect of Q_T changes (averaged over all GCM/LSMs) leads to T_S responses that are about 50% and 30% smaller (warmer), in DJF and JJA respectively, than the values that would be expected from reductions in Q_{SN} and Q_{LD} alone (Table 4). This means that if surface albedo changes were to be the only perturbation following LULCC, the ensemble of LUCID models would simulate stronger cooling in T_S (by -0.7 K and -0.5 K in DJF and JJA respectively; $\Delta_R T_S$ in Table 4). The temperature dampening is true for most models, but the magnitude of this effect varies, as do the changes in Q_T . We hypothesize, in the following, that the main cause of this dispersion resides in differences in the LSMs’ parameterizations of Q_{LE} and Q_H .

4. Attribution of the LULCC-Induced Changes to Specific Sources

[33] N2012 concluded that there are two main reasons why the various models have responses of different magnitude and even of different sign for some variables (such as latent heat flux for examples). One comes from the differences in the land-cover forcing itself. The GCM/LSMs indeed followed different rules to include the changes in crop and pasture, and thus, the nature and magnitude of imposed deforestation by the individual models between preindustrial times and present-day were quite different (Table 5). The other one comes from how LULCC affects the partitioning of Q_T between Q_{LE} and Q_H for a specific time period in the various models. N2012 however did not come to the point of quantitatively attributing the dispersion

Table 5. Forest Area Change in NAEA (10^6 km²) Between 1870 and 1992

GCM/LSM	Evergreen	Deciduous	Total
ECEARTH/TESEL	-0.3	-2.9	-3.2 (-30%)
CCAM/CABLE	-1.7	-1.0	-2.7 (-26%)
IPSL/ORCHIDEE	-1.0	-1.3	-2.3 (-22%)
SPEEDY/LPJmL	-1.4	-0.9	-2.3 (-21%)
ARPEGE/ISBA	-1.7	-0.3	-2.0 (-20%)
ECHAM5/JSBACH	-0.7	-0.5	-1.2 (-11%)
CCSM/CLM	-0.6	-0.6	-1.2 (-11%)

between the various models to one or the other source, which is what we do in the following.

4.1. How Sensitive Are the Various LSMs to LULCC?

[34] For four variables that are simulated within LSMs (α , Q_{SN} , Q_{LE} , Q_T), we have calculated their LULCC-induced changes relative to the net changes in areal fractions of the herbaceous vegetation ΔF_H (the resulting change in the fraction of crops and grasses; $\Delta F_C + \Delta F_G$) for each GCM/LSM. Figure 4 displays the resulting anomalies of each variable within each model in both DJF and JJA. Since LSMs did not include significant changes in bare soil areas, these normalized changes represent an estimate of the models responses to a hypothetical total deforestation over NAEA.

[35] Although consistent in sign, the sensitivity of α to LULCC varies in magnitude among the various models (Figure 4a), especially during the winter (DJF). In this season, the model differences roughly follow the LULCC-induced albedo changes when large snow-cover conditions

prevail (obtained from grid-cells showing monthly SWE values larger than 50 mm; indicated by crosses in Figure 4a). The albedo responses under snow are estimates of the snow-masking albedo effect. This effect is of about 0.35 when averaged over the models, in agreement with previous observational studies that compared the snow-covered surface albedos of mixed forest and herbaceous [e.g., *Jim et al.*, 2002; see also *Bonan*, 2008]. However, the individual values range between 0.27 and 0.48, revealing quite different albedo sensitivities to LULCC in snowy conditions. In addition, the differences between the simulated net α responses in DJF are larger than those obtained with large snow coverage, thereby showing that snow extent and depth at specific time periods vary significantly from one model to another, increasing the uncertainty in the responses to LULCC.

[36] The LULCC-induced albedo changes in JJA are weak compared to the DJF ones, but are likely to result in larger changes in net solar radiation at the surface due to larger incoming values, as highlighted by the normalized changes in Q_{SN} (Figure 4b). The magnitudes of Q_{SN} anomalies are generally well correlated with those of α , in spite of a few exceptions. ECHAM5/JSBACH, for instance, undergoes an increase in incoming shortwave radiation, resulting from a decrease in cloud cover (not shown), which offsets the α effect in DJF. Such behavior has already been reported for ECEARTH/TESEL in the tropics [*van der Molen et al.*, 2011].

[37] Figure 4d clearly shows that Q_T simulated for example by IPSL/ORCHIDEE is particularly sensitive to deforestation in JJA, while the same flux simulated by ECHAM5/JSBACH is insensitive to the removal of forests. Further, those models show opposite Q_{LE} responses during the same

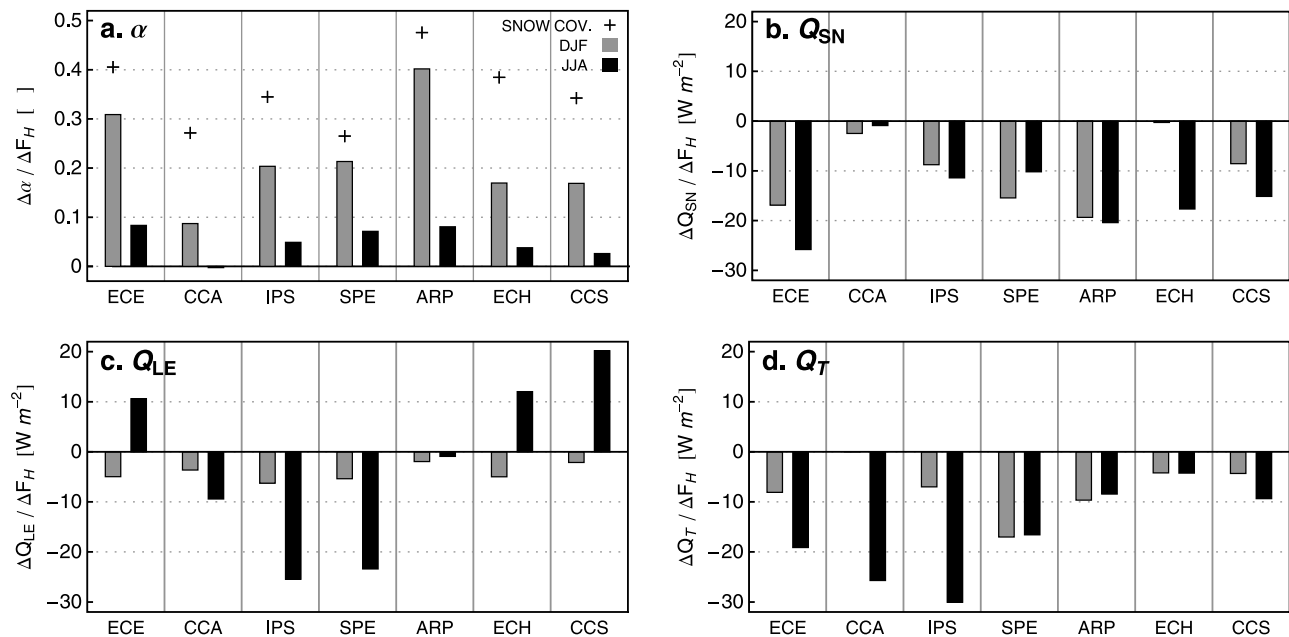


Figure 4. LULCC-induced changes in (a) surface albedo, (b) net shortwave radiation, (c) latent heat flux, and (d) total turbulent energy flux in NAEA. Anomalies normalized against the net changes in herbaceous fraction (crops + grasses/pasture, ΔF_H). Gray and black bars are for the Northern Hemisphere winter (DJF) and summer (JJA) respectively. Crosses in Figure 4a illustrate the normalized winter albedo anomalies calculated from grid-cells within NAEA showing large snow content ($SWE > 50$ mm). Model acronyms are the same as in Figure 3.

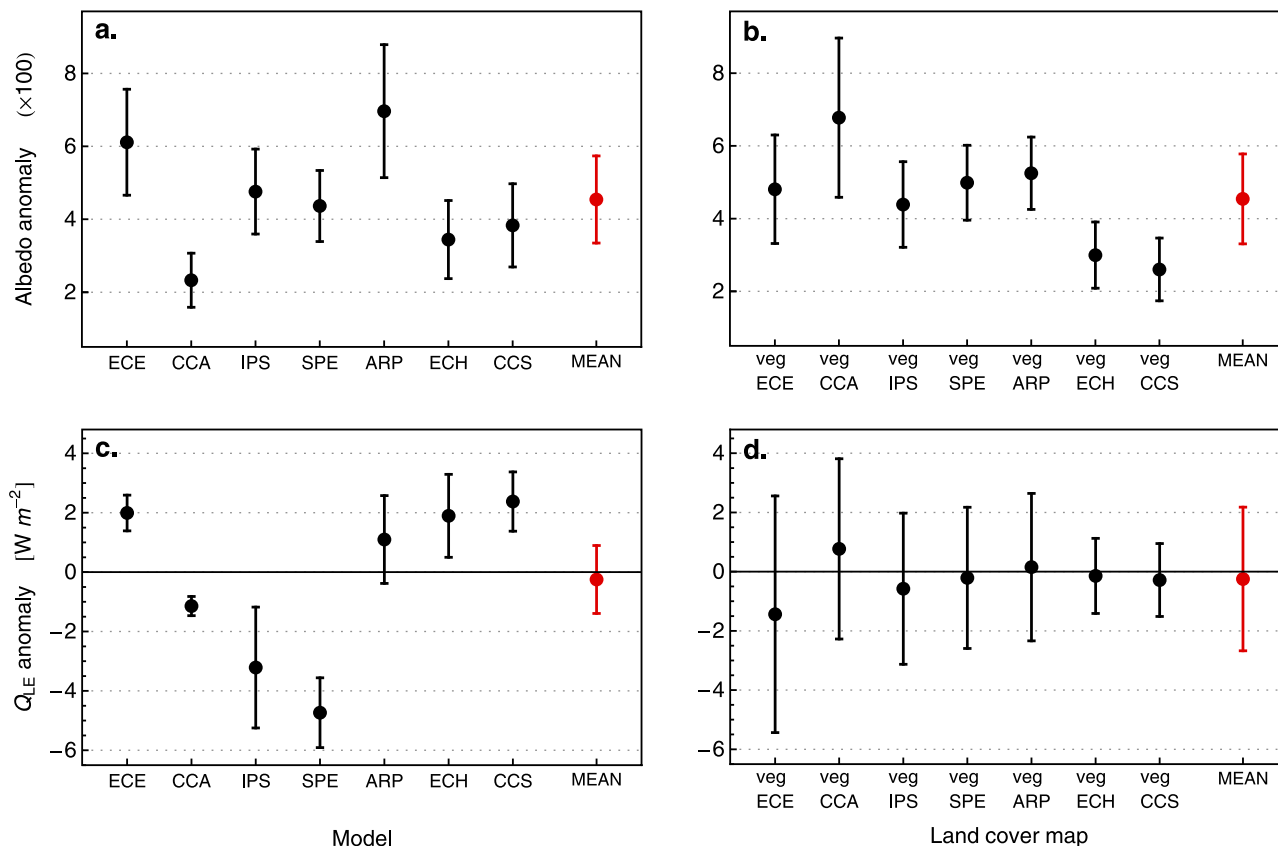


Figure 5. Reconstructed LULCC-induced changes in (a and b) surface albedo in DJF and (c and d) latent heat flux in JJA. Calculations are done for the seven LUCID GCM/LSMs and their specific land cover maps in NAEA. Figures 5a and 5c illustrate the mean response of each model and the ± 1 mean deviation (MD) associated to various land-cover forcings. The length of each error bar therefore represents the sensitivity of each GCM/LSM to the various vegetation maps tested. Figures 5b and 5d show mean response associated to each land-cover map and the spread resulting from the choice of GCM/LSM. Veg‘MOD’ stands for the land-cover map of the specific model. Model acronyms are the same as Figure 3.

season (Figure 4c). It is also clear that one model may have a relatively (to other models) strong response in one variable (e.g., IPSL/ORCHIDEE for Q_{LE} or Q_T) and a relatively weak response in another one (same model for Q_{SN}). Quantifying the robust impacts of LULCC on climate from our simulations is therefore complicated by the wide range of sensitivities the LSMs display to LULCC. As noted by N2012, this highlights the need to evaluate LSMs by examining how they respond to a perturbation in addition to how they simulate an average state.

[38] Figure 4d therefore shows large differences between the models in ΔQ_T as a function of ΔF_H for individual seasons, while N2012 tended to conclude, from their Figure 12, that ΔQ_T was rather proportional to the magnitude of deforestation. This may be true at the annual timescale but is certainly wrong at the seasonal one. LSMs therefore also diverge in estimating how Q_T responds to LULCC, and not only in the way they partition Q_T and its changes between Q_{LE} and Q_H , as N2012 tended to conclude.

4.2. Relative Contributions of Land Cover Map and Model Sensitivity to the Inter-model Variability

[39] We used a multivariate regression analysis (section 2) to attribute the dispersion between the individual models’

response to LULCC either to (a) the differences in land-cover changes since preindustrial times or to (b) the parameterizations included in the individual models that lead to different sensitivities to land cover perturbations. For the three variables assessed in this analysis (α , Q_{LE} and Q_T), the regression models allow an evaluation of parameterization differences between the various GCM/LSMs (represented by the regression coefficients) and of differences in land cover forcing. For each GCM/LSM we reconstructed the responses to LULCC in NAEA, and each model was forced with each of the seven alternative land-cover maps. The set of 7 (models) by 7 (land-cover patterns) reconstructions were evaluated with a common (model-mean) perturbation of the environmental drivers (snow content, precipitation and net short-wave radiation; see Table 2) to avoid including potential differences that would result from ranges in the climate forcing itself. In order to minimize the effect of outliers, we use the simple mean deviation (MD) statistic (i.e., the average of the absolute deviations of series elements from the series mean) as a spread measure instead of the more typical standard deviation.

[40] Figure 5 shows the reconstructed responses to LULCC for two sensitive cases: α in DJF and Q_{LE} in JJA. The LULCC-induced anomalies are illustrated in two ways (Figures 5a

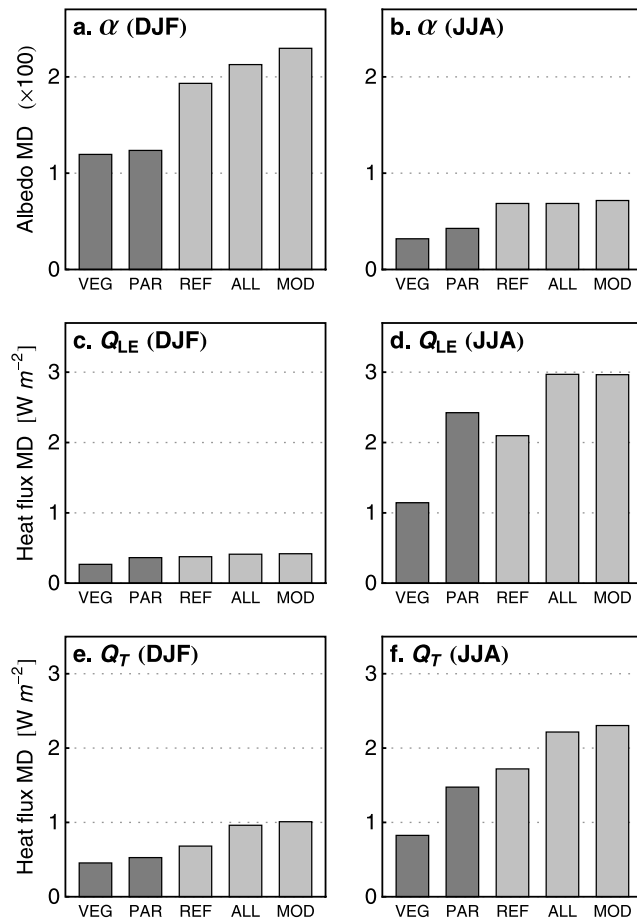


Figure 6. Inter-model mean deviation (MD) of the computed seasonal LULCC-induced anomalies (GCMs-based statistical reconstructions) of (a and b) surface albedo, (c and d) latent heat, and (e and f) total turbulent heat flux in NAEA. Bars VEG and PAR illustrate the estimated inter-model spread induced by respectively the different land-cover forcings and the different land-surface parameterizations (see Figure 5). REF indicates the MDs accounting simultaneously for VEG and PAR. Reconstructions VEG, PAR and REF are forced by common (model-mean) changes in the environmental predictors (see text). ALL indicates the MDs resulting from the fully reconstructed responses (accounts simultaneously for VEG and PAR and the individual model changes in environmental predictors). Differences between REF and ALL result therefore from the LULCC-induced environmental changes in each GCM/LSM. MOD illustrates the MDs between the responses simulated by the GCM/LSMs.

and 5c on one hand, and Figures 5b and 5d on the other). Figures 5a and 5c show the average responses of α and Q_{LE} reconstructed for each GCM/LSM and their associated variation (± 1 MD) resulting from various land-cover forcing-derived responses. To construct these figures, each statistical model derived for a given GCM/LSM has been driven by the land-cover forcing of all individual GCM/LSMs. Thus, the error bar length (2 MD) is an estimate of how different the albedo (or the latent heat flux) anomaly would be had a given GCM/LSM used the land-cover forcing from another GCM/LSM.

[41] In turn, Figures 5b and 5d show the mean α and Q_{LE} responses reconstructed for each of the imposed LULCC maps and their resulting dispersion associated to the various model-derived results. The error bar length indicate in this case an estimate of how different the individual LSMs respond to the same land-cover forcing (e.g., vegECE refers to the reconstructed responses of all models to the land-cover forcing of ECEARTH/TESSSEL). In all figures, the final value (labeled as MEAN) indicates the mean of the means (the resulting model-mean response of the concerned variable) and the corresponding error bar is the mean of the MDs (i.e., in Figures 5a and 5c, this represents the mean spread induced by the different land-cover maps). These averaged MDs have been re-plotted in Figure 6 and labeled as VEG to illustrate the multi-model spread component related to the various land-cover forcings (as those shown in Figures 5a and 5c), and labeled PAR to represent the mean spread resulting from the various LSMs parameterizations (as those shown in Figures 5b and 5d).

[42] The reconstructed anomalies of α and Q_{LE} highlight the different sensitivities to LULCC shown by the LUCID GCM/LSMs (Figures 5a and 5c) and agree with the results shown in Figure 4. Particularly, in the Q_{LE} case, the mean values reproduce the inherent responses to LULCC of each model (e.g., clearly negative in the case of IPSL/ORCHIDEE and SPEEDY/LPJmL, or positive in the case of ECEARTH/TESSSEL and CCSM/CLM; dots in Figure 5c). Further, the MD values show that some models are fairly insensitive in their Q_{LE} responses to the differences between the imposed LULCC (ECEARTH/TESSSEL, CCAM/CABLE and CCSM/CLM), while others show quite different amplitudes (IPSL/ORCHIDEE). For some models such as CCSM/CLM for example, the positive “mean” Q_{LE} response can be traced back to the way the CLM LSM calculates latent heat flux and more specifically the contribution, to total evapotranspiration, of soil evaporation, canopy interception and transpiration. *Lawrence and Chase* [2009] have qualified this evapotranspiration partitioning in this version of CLM as “inconsistent”, and have concluded that changing this partitioning may have significant consequences on climate modeling experiments investigating the influence of LULCC.

[43] In Figures 5b and 5d, the land-cover forcing in the x-axis is sorted by decreasing amount of deforestation (from that prescribed in ECEARTH/TESSSEL (vegECE) to that of CCSM/CLM (vegCCS); see Table 5). As expected, the mean responses and the associated spread are quite small when LULCC is small (i.e., all the models show weak responses when evaluated with the land cover of ECHAM5/JSBACH and CCSM/CLM), and increase with the magnitude of deforestation. One clear exception can be seen for α in DJF (Figure 5b): the larger response occurs when the models are forced with land cover maps of CCAM/CABLE (vegCCA) rather than those of ECEARTH/TESSSEL (vegECE). This results from the type of forest that has been removed at the expense of crops and pasture. Deciduous forests are mainly decreased in TESSSEL while in CABLE the largest decrease is in evergreen trees (Table 5), thereby inducing a larger change in snow-masking effect during the winter.

[44] The MD between the various model responses of α and averaged over the seven land cover patterns (MEAN error bar in Figure 5b) are almost identical to the averaged MD that

measures the spread between the various land-cover forcings (MEAN error bar in Figure 5a), showing that both the land cover forcing strength and the model sensitivity to LULCC play a similar role in explaining the final inter-model spread in the winter albedo responses. In contrast, for the summer Q_{LE} case, the mean spread related to the inherent responses of the models (MEAN error bar in Figure 5d) is clearly larger than the one related to the different LULCC forcing (Figure 5c), indicating a stronger role of the model's parameterizations in the resulting net inter-model spread.

[45] The averaged MDs illustrated in Figure 5 and those related to the other variables assessed (α , Q_{LE} and Q_T , in DJF and JJA) are summarized in Figure 6. As indicated above, VEG bars represent the contribution to the dispersion among the various models' responses to LULCC of the different magnitudes of LULCC, while PAR illustrates the contribution of the various model parameterizations. As a reference for these two quantities, the resulting MD between the individual model responses reconstructed with their corresponding land-cover forcings, but using a common perturbation in the environmental predictors (same as used in VEG and PAR reconstructions), is also illustrated in Figure 6 (labeled as REF). Further, values indicated as ALL and MOD in Figure 6 show the inter-model MDs of the fully reconstructed responses (including the individual environmental drivers) and of the simulated responses (from the GCM/LSMs), respectively.

[46] As already stated, for α in DJF or Q_{LE} in JJA, the LSM parameterizations play a role as important as the LULCC strength in explaining the differences between the model responses to LULCC. In general, the MD associated to the various land-surface forcings (VEG) is of the same order of magnitude, but often lower than PAR, particularly for the summer (JJA) responses of Q_{LE} and Q_T (Figure 6). While VEG and PAR are not identical, accounting for both simultaneously (REF bars) explains more than 75% of the MD resulting from the fully reconstructed responses (ALL) or the simulated responses (MOD). In the case of α and Q_T , both VEG and PAR generate less dispersion than REF in DJF and JJA, showing that those two sources of dispersion are additive, increasing the final spread. For the JJA Q_{LE} case, there is some compensatory effect and the spread induced by PAR is slightly greater than that obtained in REF. The differences between REF and ALL result from the LULCC-induced atmospheric changes in each GCM/LSM; i.e., atmospheric feedbacks amplify the Q_{LE} responses to LULCC, increasing the resulting inter-model spread (see section 4.3).

4.3. Attribution of LULCC Responses to Various Drivers

[47] Given that more than 50% of the inter-model dispersion in the responses of α , Q_{LE} and Q_T is explained by the different GCM/LSM sensitivities to LULCC, we have used our statistical models to evaluate the nature of the model responses and to estimate the contribution of the various drivers assessed. For each GCM/LSM and each variable (α , Q_{LE} and Q_T) we have therefore calculated the LULCC-induced variation components of their different predictors (Figure 7). To highlight the inherent model differences, the reconstructed responses to LULCC were normalized with the corresponding change in F_H , as was done for Figure 4.

[48] Since the regression model of α explicitly separates the snow-free and the snow-covered albedos (see Appendix A), the changes of this variable can be attributed to both quantities. In all models, the LULCC-induced winter (DJF) α anomalies are clearly led by the changes in its snow-covered component, which represents the change in canopy snow-masking effect (Figure 7a). The latter can be induced by changes in vegetation partitioning (F_v ; dark grey bars in Figure 7a) and/or by changes in the LAI for a given vegetation type (light grey bars). The type of response varies across the models: IPSL/ORCHIDEE and SPEEDY/LPJmL respond only to perturbations in F_v , while the rest also show a contribution of LAI changes. Changes in the snow content (SWE) represent an indirect impact of LULCC that could result from a positive feedback between temperature, snowpack and α (i.e., snow-albedo feedback). The sign of simulated SWE changes are consistent with this, but do not represent a significant contribution to the overall α responses (indicated with white bars in Figure 7a), and is only noticeable in some models (e.g., ECEARTH/TESEL). The snow-free-related α changes also play a secondary role during the winter (green bars). Although different in amplitude, the α responses in DJF of the various models are quite similar in their form and are dominated by snow and foliage projected cover. This confirms the conclusions of N2012 that the main processes behind the changes in α are coherent between models.

[49] The summer (JJA) α responses to LULCC are driven by differences in the snow-free optical properties of the various land cover types (F_v), and by changes in LAI (the contributions of both drivers are displayed together in Figures 7 and 8). CCAM/CABLE shows a negligible α anomaly in JJA because this version of the model does not distinguish leaf/stem albedos between PFTs. The other models show an averaged snow-free α response of about 0.05, in agreement with observed snow-free albedo differences between herbaceous and forest [Jin *et al.*, 2002], but – as for the snow covered case – with significant differences between the individual results (ranging from 0.025 to 0.08).

[50] The results are clearly less uniform in the Q_{LE} case in JJA (Figure 7d). First, all drivers play a significant role explaining the LULCC-induced changes of this variable. Second, the scale of explanation varies greatly between models in both magnitude and sign. The anomalies induced by perturbations in the vegetation partitioning (F_v) and LAI are mainly responsible for the model differences in the overall Q_{LE} responses. Although different in sign, the precipitation-induced Q_{LE} anomalies (the contribution of both drivers R and R- are shown together; blue bars in Figure 7d) show a similar contribution between the models when compared to the precipitation changes themselves (see Figure 8b). In addition, the LULCC-induced precipitation anomalies in JJA are closely proportional to the Q_{LE} ones when compared between the models (not shown). These patterns show that the impacts of LULCC on Q_{LE} and precipitation are not independent and, on the contrary, suggest a coupling and positive feedback between these variables of similar intensity between the models. This agrees with previous studies that identify a positive soil moisture-evapotranspiration feedback in the Northern Hemisphere temperate regions [Koster *et al.*, 2004; Seneviratne *et al.*,

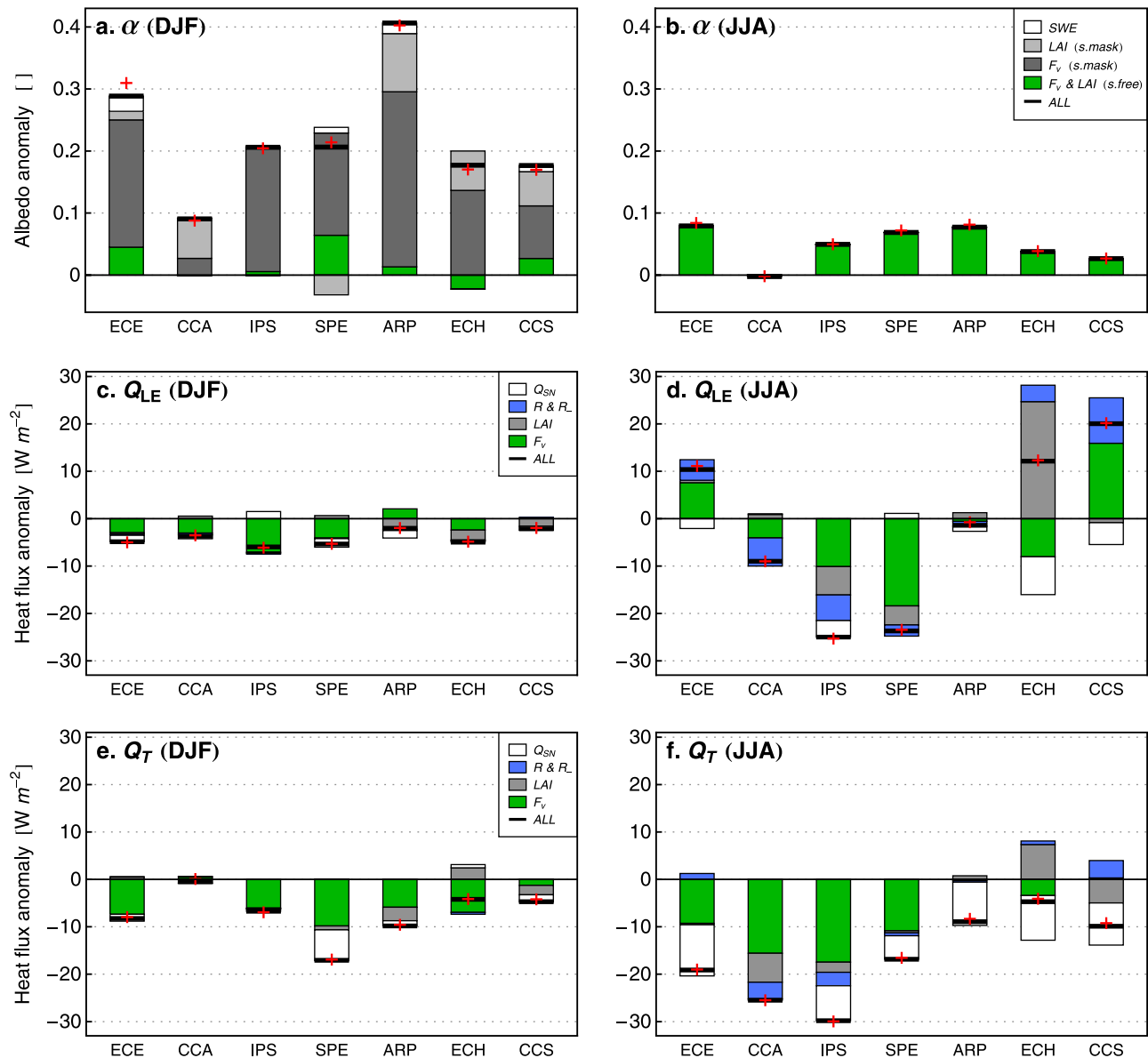


Figure 7. Reconstructed seasonal LULCC-induced anomalies of (a and b) surface albedo, (c and d) latent heat flux, and (e and f) total turbulent flux in NAEA. As for Figure 4, the anomalies are normalized with the corresponding change in herbaceous area (ΔF_H). Stacked bars illustrate the contribution from different drivers used in the corresponding multivariate analysis (Table 2). Red crosses indicate the LULCC-induced anomalies in the concerned variable simulated by the GCM/LSMs. Model acronyms are the same as Figure 3.

2010]. Except for SPEEDY/LPJmL, the Q_{LE} anomalies induced by shortwave radiation changes are also consistent between the models, with values approximately proportional to the Q_{SN} perturbations (white bars in Figure 7d).

[51] In the case of CCSM/CLM, the reconstructed Q_{LE} anomalies seem to underestimate the LAI effect against the contribution of F_v (this is not a surprise given the large spatial covariability between forest fraction and LAI in this model, Table 3). However, as already discussed in section 4.2, the contribution to total evapotranspiration of various soil-plant parts in this model is incorrect [Lawrence and Chase, 2009]. The JJA Q_{LE} response is largely explained by a significant increase of soil evaporation (resulting from

both the decrease in canopy density and the increased amount of rainfall reaching the ground) largely counteracting the drop in canopy interception and transpiration, and therefore reducing the sensitivity of Q_{LE} to LULCC. For other models such as ECHAM5/JSBACH, IPSL/ORCHIDEE and SPEEDY/LPJmL, LAI is an important driver in the Q_{LE} responses. As discussed in N2012, these three models are the only ones that do compute LAI on-line, as a function of biomass allocation. They show quite different seasonal LAI responses to LULCC resulting from their discrepancy in the way they parameterize the phenological cycle of crops compared to the other vegetation types. For example, the resulting LULCC-induced LAI anomaly in JJA is positive in

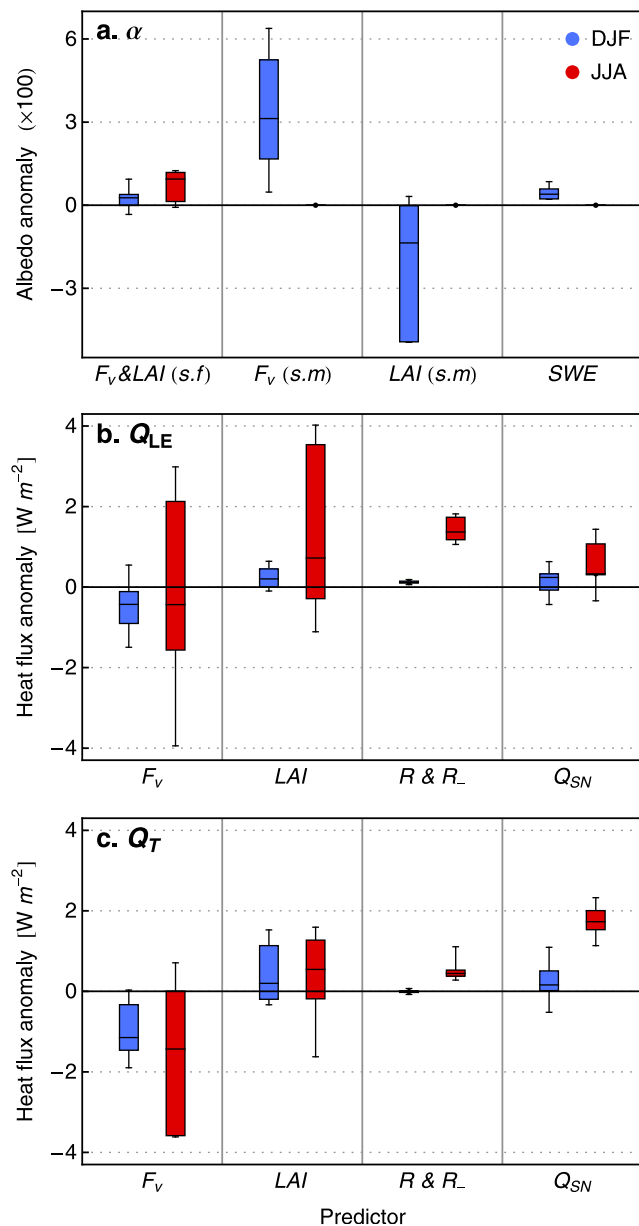


Figure 8. DJF (blue) and JJA (red) anomalies of (a) surface albedo, (b) latent heat flux, and (c) total turbulent flux in NAEA expected from changes in each of the corresponding predictors (see Table 2). The abbreviations s.f and s.m in Figure 8a indicate respectively the snow-free and the snow-covered components of the surface albedo calculations. All the LUCID GCMs-based statistical models were forced with a common set of perturbations (most of the used predictor's changes are positives; shown in Table 6). Box-whisker plots indicate the extremes, the inter-quartile and the median within the individual (GCMs-based) results.

the case of ECHAM5/JSBACH and negative in the cases of IPSL/ORCHIDEE and SPEEDY/LPJmL (not shown).

[52] The LULCC-induced Q_T anomalies are dominated by the changes in F_v and Q_{SN} for five out of seven models (Figures 7e and 7f). Exceptions are ECHAM/JSBACH and CCSM/CLM that are more sensitive to LAI changes than to F_v changes, especially during summer time. As for Q_{LE} , the

JJA Q_T anomalies driven by Q_{SN} are proportional to the Q_{SN} perturbations themselves, and are coherent with the expected radiative impacts of LULCC in Q_T (Figure 3). The Q_T anomalies induced by precipitation in JJA, although quite small, show a similar pattern with those obtained in the Q_{LE} analysis, suggesting a positive impact of Q_{LE} on Q_T in all models (i.e., more/less rainfall leads to more/less Q_{LE} and thereby more/less Q_T). In most models, the non-radiative drivers (i.e. LAI and F_v) cause negative Q_T anomalies, confirming our discussion in section 3. Part of the negative contribution that changes the land-surface partitioning (F_v) exerts on the DJF and JJA Q_T responses can probably be attributed to decreases in surface roughness (Z_0), as discussed in Davin and de Noblet-Ducoudré [2010].

5. Discussion and Conclusions

[53] This paper extends the study of Pitman *et al.* [2009] and de Noblet-Ducoudré *et al.* [2012] that investigated the robust responses of the surface climate to the land-use induced land-cover change (LULCC) since pre-industrial times, using a coordinated set of experiments carried out by seven GCM/LSMs. Apart from reassessing some previous findings, we have quite thoroughly explained why the models show different responses to LULCC in the Northern Hemisphere temperate regions, and quantified the contribution of various drivers to the simulated inter-model spread.

[54] LUCID models simulate systematic decreases in net solar radiation in all seasons, mainly produced by an increase in the snow-free surface albedo and a reduction in the snow-masking albedo effect during winter. We show that the expected radiatively induced cooling is significantly dampened (and sometimes offset) by a decrease in the total turbulent energy flux, which is mainly driven by changes in land-cover properties other than canopy albedo (e.g., surface roughness). Although all the models show consistent signs for both radiative and non-radiative impacts on surface temperatures (respectively cooling and warming), their magnitude varies significantly, resulting in quite different net changes in surface temperature.

[55] One cause of discrepancy in the models' responses to LULCC results from the way individual LSMs have implemented land-use changes in their own land-cover map. For example, the resulting differences in biogeography explain about one third of the inter-model dispersion in the summer latent heat flux responses, and about one half in the winter albedo ones. This is quite significant compared to the contribution of the inherent model sensitivities to LULCC. Our quantification confirms the hypothesis set forward by Pitman *et al.* [2009] and de Noblet-Ducoudré *et al.* [2012]: they argue that reducing the inter-model spread in its responses to LULCC will imply that modelers do agree on common maps or, *a minima*, on methodologies to implement land-use changes. This could not be done before the coordinated set of CMIP5 experiments and, therefore, models may diverge in their regional response to LULCC due to discrepancies in their land-cover maps.

[56] One important conclusion of this study lies in the major role that the models' sensitivity to land-cover perturbations plays in the resulting climate impacts of LULCC. Within the LUCID models, the dispersion resulting from the different land-surface parameterizations is either comparable

Table 6. Predictors' Changes in DJF and JJA Used in the Statistical Models (Table 2) to Evaluate the GCMs Sensitivities (Illustrated in Figure 8)^a

Season	ΔF_c	ΔF_g	ΔF_e	ΔF_d	ΔLAI	ΔSWE (mm)	ΔR (mm)	ΔR_- (mm)	ΔQ_{SN} (W m ⁻²)
DJF	0.26	-0.06	-0.10	-0.10	0.30	1.54	3.4	4.8	2.6
JJA	0.26	-0.06	-0.10	-0.10	0.33	0.0	7.9	5.0	3.7

^aThe anomalies correspond to the mean (inter-model) of the absolute LULCC-induced changes in NAEA, except for those used for the land cover fractions F_v (F_c , F_g , F_e , F_d), which correspond to the simple means.

to (e.g., the surface albedo case) or quite larger than (e.g., in latent heat flux case) the one resulting from differences in the imposed land-cover (Figure 6). These different sensitivities that can be appreciated in Figures 4–7, are particularly explicit in Figure 8. This figure illustrates the surface albedo (α), latent heat flux (Q_{LE}) and total heat flux (Q_T) changes in NAEA, expected (reconstructed) in the various models, but induced by identical perturbations (most of them positives). Apart from the change in the land cover partitioning (F_v) that was set to the model-mean LULCC (i.e., deforestation), those perturbations are the model-mean of the absolute changes (in the corresponding drivers) induced by LULCC (see Table 6). Figure 8 therefore highlights the models' consistencies and divergences resulting from their different land-surface parameterizations and land-atmosphere coupling intensities. For instance, the LUCID models clearly agree in the magnitude of the summer Q_T and Q_{LE} increases, in responses to increases in respectively net solar radiation (Q_{SN}) and precipitation (R and R_-). Most models also show consistent signs in their α responses to LAI and F_v changes, or in their Q_T responses to F_v . In these cases, however, the models exhibit quite different amplitudes in their responses. It is also clear how different the model Q_{LE} responses to a common change in F_v and in LAI are during the summer, drivers that are therefore behind the uncertainties in the simulated LULCC-induced anomalies of this flux.

[57] As discussed by *de Noblet-Ducoudré et al.* [2012], the differences displayed by the LUCID models highlight the need to improve benchmarking tools for LSMs evaluation. These tools need to evaluate the capacity of the LSMs to simulate the mean climate, but also assess how LSMs respond, for example, to a land-cover perturbation. LSMs evaluation needs to be undertaken in uncoupled (off-line) simulations, but also needs to extend to the examination of processes in land-atmosphere coupled runs that capture the feedbacks between the land and atmosphere and account for differences in the coupling strength between these components [e.g., *Koster et al.*, 2004].

[58] Changes in the surface albedo, latent heat and total turbulent heat flux induced by LULCC were assessed through a multivariate statistical analysis. An important concern regarding the used method, as well as with all other techniques that measure covariability between data, is that these do not ensure causality between explanatory variables and predictands. Our assumption is that the selected predictors (land-cover types, leaf area index, snow content, precipitation and solar radiation) very likely explain the bulk of the spatial and temporal variability of the assessed variables, and are the main contributors to the LULCC-induced impacts on these variables. Taking into account this concern, the partial contribution of each predictor (as is shown in Figures 7 and 8) should be interpreted carefully, since it could be underestimated or overestimated depending on the

co-linearity with another predictor (e.g., land-cover fractions and LAI) or with another important driver not considered here (e.g., wind speed). Nevertheless, the purpose of this analysis is to estimate and compare (model-by-model) the sensitiveness of the assessed predictands to perturbations in the corresponding drivers in a common framework, rather than to measure the exact contribution of each of these drivers (for which other ad-hoc simulations would be needed).

Appendix A: Multivariate Regression Analysis

A1. Regression Models

[59] As introduced in section 2 and presented in section 4, a multivariate statistical analysis was performed to mimic the LULCC-induced anomalies shown by the LUCID models in the NAEA in three variables: surface albedo (α), latent heat flux (Q_{LE}) and total turbulent energy flux (Q_T). Seasonal anomalies of these variables were regressed upon a selected number of drivers, including the land cover partitioning (represented by the surface area fraction of five land-cover types) within NAEA (Table 2). The regression models follow equation (5). The climatological means (\bar{Y}_v) and the anomalies (Y'_v) are estimated as first and second order polynomial expansions over the various predictors included in \mathbf{P} . That is,

$$\bar{Y}_v(\mathbf{P}) = a_v + \sum_{i=1}^n b_v^{(i)} \bar{P}_i \quad (\text{A1})$$

$$Y'_v(\mathbf{P}) = \sum_{i=1}^n c_v^{(i)} P'_i + \sum_{i=1}^n \sum_{j=1}^n d_v^{(i,j)} \bar{P}_i P'_j \quad (\text{A2})$$

where n is the \mathbf{P} length. These two expressions define the sets of coefficients a_v , $b_v^{(i)}$ and $c_v^{(i)}$ and $d_v^{(i,j)}$ which are computed for each GCM/LSM using linear routines. The standard least squares method was used to minimize the difference between the expected predictands values and those simulated by the LUCID models. These parameters represent the partial derivatives of \bar{Y}_v and Y'_v with respect to the various predictors. The mean states \bar{P}_i were included as second-order predictors (the second term on the right-hand side of equation (A2)) to improve the effect of some non-linear dependencies of Y'_v .

[60] The analyses were performed for each season separately (only the winter and summer results are shown here) and, since most of the used drivers vary in time and space, the input data (predictors and predictands) were conformed by the multiannual seasonal values of all grid-cells within the NAEA region. In order to have a coherent domain and a good representation of the regional means, the GCM/LSM fields were previously interpolated to a common rectangular

Table A1. Coefficients of Determination (r^2) Between the Predicted and the Simulated Seasonal Anomalies of Surface Albedo (α), Latent Heat Flux (Q_{LE}) and Total Turbulent Heat Flux (Q_T)^a

GCM/LSM	α		Q_{LE}		Q_T	
	DJF	JJA	DJF	JJA	DJF	JJA
EARTH/TESEL	0.86 (0.99)	0.96 (1.00)	0.49 (0.77)	0.76 (0.90)	0.36 (0.54)	0.84 (0.94)
CCAM/CABLE	0.85 (0.91)	0.68 (0.98)	0.41 (0.65)	0.84 (0.90)	0.25 (0.17)	0.78 (0.92)
IPSL/ORCHIDEE	0.83 (0.96)	0.72 (0.99)	0.40 (0.57)	0.89 (0.94)	0.23 (0.45)	0.88 (0.98)
SPEEDY/LPJmL	0.78 (0.95)	0.87 (0.98)	0.50 (0.69)	0.80 (0.90)	0.73 (0.84)	0.84 (0.87)
ARPEGE/ISBA	0.88 (0.99)	0.92 (0.99)	0.39 (0.35)	0.71 (0.81)	0.22 (0.40)	0.83 (0.87)
ECHAM5/JSBACH	0.76 (0.92)	0.45 (0.97)	0.45 (0.51)	0.77 (0.85)	0.19 (0.33)	0.87 (0.88)
CCSM/CLM	0.86 (0.97)	0.68 (0.80)	0.37 (0.30)	0.78 (0.89)	0.18 (0.11)	0.87 (0.84)

^aValues calculated with the entire data (i.e., r^2 measures the spatial and temporal covariability), and with the regional mean (averaged over NAEA) time series (in brackets).

$2^\circ \times 2^\circ$ latitude-longitude grid, and the regressions were computed using area-equivalent weighted values.

A2. Surface Albedo

[61] In the case of the surface albedo (α), the regression model was defined as a semi-empiric function in order to separate the albedo under snow (α_s) and the snow-free component (α_{sf}). The resulting net albedo of a grid-cell was therefore derived from the snow-covered area fraction of the cell, i.e.,

$$\alpha = (1 - f_s)\alpha_{sf} + f_s\alpha_s \quad (A3)$$

$$f_s = 1 - e^{-kSWE} \quad (A4)$$

The snow-cover fraction (f_s) was defined as an asymptotic function of the snow content (SWE). The convergence coefficient k is estimated for each model in a separated non-linear regression analysis.

[62] Keeping the first order terms when using perturbed forms of α_s , α_{sf} and f_s in equation (A3), we obtain the total albedo anomaly (α') used in the analysis:

$$\alpha' = (1 - \bar{f}_s)\alpha'_{sf} + \bar{f}_s\alpha'_s + f'_s(\bar{\alpha}_s - \bar{\alpha}_{sf}). \quad (A5)$$

[63] The first and second term in the right hand of equation (A5) represents the components of α' related to changes in the snow-free albedo and in the snow-covered albedo respectively, while the last term represents the contribution from a change in the snow-covered area. Equation (A5) was further generalized to each land-cover type and used to calculate the grid-mean values following equations (4) and (5). The land-cover type components of α_s and α_{sf} were therefore defined empirically as those of Q_{LE} and Q_T (equations (A1) and (A2)), using LAI as a single predictor.

A3. Regression Results

[64] We do not find significant autocorrelations within the interannual series of the variables assessed that could induce to misleading interpretation of the results. However, as pointed out in sections 2 and 5, the used explanatory variables are not statistically independent in some cases, mainly because the coherent spatial variability between them. One

clear example of that occurs between the land cover fractions (F_V) and LAI . LAI was included in the analyses because the predictability of the statistical models is significantly enhanced, but for GCMs such CCSM (that show a strong correlation between forest fraction and LAI ; Table 3), the particular contribution of this predictor to the expected responses is not reliable and must be taken in account together with the one of F_V .

[65] A synthesis of the regression analyses results is presented in Table A1 for DJF and JJA. The skill of the regression models are evaluated through the resulting coefficients of determination (r^2) between the predicted values of α' , Q'_{LE} and Q'_T and the corresponding anomalies simulated by the GCM/LSMs. Two r^2 calculations are indicated in Table A1, computed respectively with the entire record of the concerned variable (i.e., accounting for the spatial and temporal covariability) and with the regional mean (NAEA) time series (shown in brackets).

[66] In the case of the surface albedo, the estimates fit comparatively well with the simulated values in both DJF and JJA, explaining about 80% of the α' variance. The reconstructed regional mean series of α' are better represented, with r^2 values greater than 0.9 in most cases and near 1.0 in several models. The predicted JJA series of Q'_{LE} and Q'_T also account for about 80% of the variance of the simulated values. In turn, the estimates of this two predictands are significantly worse in DJF, indicating that during the winter there are other significant drivers controlling the turbulent heat exchanges not considered in these analyses, notably wind speed.

[67] Besides the statistical model's skill to predict the analyzed variables, the utility of this method resides in the ability to represent the GCM/LSM responses to LULCC. The reconstructed seasonal responses of α , Q_{LE} and Q_T were calculated in NAEA from the predicted mean fields of each experiment (Table 1), and then evaluated using equation (1). As Figure 7 illustrates, the resulting anomalies in DJF and JJA fit closely those simulated by the GCM/LSMs in the three assessed variables, showing that the perturbations in the selected drivers explain the changes induced by LULCC.

[68] **Acknowledgments.** The authors are grateful to all LUCID participants for providing modeling data and supporting this research, as well as for three anonymous reviewers for their constructive comments. We also acknowledge the inspiring discussions, input and collaboration between the participants of the LULCC initiative, IGBP 2nd Synthesis topic on 'Land-Use-induced Land-Cover Changes and the functioning of the Earth

System'. JPB thanks the grant support from the Chilean National Commission for Scientific and Technological Research (CONICYT). The computing time was provided by the Commissariat à l'Énergie Atomique (CEA), France.

References

- Abramowitz, G. (2005), Towards a benchmark for land surface models, *Geophys. Res. Lett.*, *32*, L22702, doi:10.1029/2005GL024419.
- Abramowitz, G., R. Leuning, M. Clark, and A. Pitman (2008), Evaluating the performance of land surface models, *J. Clim.*, *21*, 5468–5481.
- Baldocchi, D. D., C. A. Vogel, and B. Hall (1997), Seasonal variation of energy and water vapor exchange rates above and below a boreal jack pine forest canopy, *J. Geophys. Res.*, *102*(D24), 28,939–28,951.
- Betts, R. A. (2001), Biogeophysical impacts of land use on present-day climate: Near surface temperature and radiative forcing, *Atmos. Sci. Lett.*, *1*, 39–51, doi:10.1006/asle.2001.0023.
- Betts, R. A., P. D. Falloon, K. Klein Goldewijk, and N. Ramankutty (2007), Biogeophysical effects of land use on climate: Model simulations of radiative forcing and large-scale temperature change, *Agric. For. Meteorol.*, *142*, 216–233.
- Bonan, G. B. (2008), Forests and climate change: Forcings, feedbacks, and the climate benefits of forests, *Science*, *320*, 1444–1449, doi:10.1126/science.1155121.
- Bondeau, A., et al. (2007), Modelling the role of agriculture for the 20th century global terrestrial carbon balance, *Global Change Biol.*, *13*(3), 679–706.
- Bounoua, L., R. DeFries, G. J. Collatz, P. Sellers, and H. Khan (2002), Effects of land cover conversion on surface climate, *Clim. Change*, *52*, 29–64.
- Butt, N., P. A. de Oliveira, and M. H. Costa (2011), Evidence that deforestation affects the onset of the rainy season in Rondonia, Brazil, *J. Geophys. Res.*, *116*, D11120, doi:10.1029/2010JD015174.
- Collins, W. D., et al. (2006), The Community Climate System Model Version 3 (CCSM3), *J. Clim.*, *19*, 2122–2143.
- Davin, E. L., and N. de Noblet-Ducoudré (2010), Climatic impact of global-scale deforestation: Radiative versus non radiative processes, *J. Clim.*, *23*, 97–112.
- Davin, E. L., N. de Noblet-Ducoudré, and P. Friedlingstein (2007), Impact of land cover change on surface climate: Relevance of the radiative forcing concept, *Geophys. Res. Lett.*, *34*, L13702, doi:10.1029/2007GL029678.
- de Noblet-Ducoudré, N., et al. (2012), Determining robust impacts of Land-Use induced Land-Cover Changes on surface climate over North America and Eurasia: Results from the first of LUCID experiments, *J. Clim.*, *25*, 3261–3281.
- Ellis, E. C., K. Klein Goldewijk, S. Siebert, D. Lightman, and N. Ramankutty (2010), Anthropogenic transformation of the biomes, 1700 to 2000, *Global Ecol. Biogeogr.*, *19*, 589–606, doi:10.1111/j.1466-8238.2010.00540.x.
- Feddema, J., K. Oleson, G. Bonan, L. Mearns, L. E. Buja, G. A. Meehl, and W. M. Washington (2005a), The importance of land-cover change in simulating future climates, *Science*, *310*, 1674–1678.
- Feddema, J., K. Oleson, G. Bonan, L. Mearns, W. Washington, G. Meehl, and D. Nychka (2005b), A comparison of a GCM response to historical anthropogenic land cover change and model sensitivity to uncertainty in present-day land cover representations, *Clim. Dyn.*, *25*, 581–609.
- Forster, P., et al. (2007), Changes in atmospheric constituents and in radiative forcing, in *Climate Change 2007: The Physical Science Basis. Contribution of Working Group I to the Fourth Assessment Report of the Intergovernmental Panel on Climate Change*, edited by S. Solomon et al., pp. 129–234, Cambridge Univ. Press, Cambridge, U. K.
- Georgescu, M., D. B. Lobell, and C. B. Field (2011), Direct climate effects of perennial bioenergy crops in the United States, *Proc. Natl. Acad. Sci. U. S. A.*, *108*, 4307–4312, doi:10.1073/pnas.1008779108.
- Gero, A. F., A. J. Pitman, G. T. Narisma, C. Jacobson, and R. A. Pielke (2006), The impact of land cover change on storms in the Sydney Basin, *Global Planet. Change*, *54*, 57–78, doi:10.1016/j.gloplacha.2006.05.003.
- Govindasamy, B., P. B. Duffy, and K. Caldeira (2001), Land use changes and Northern Hemisphere cooling, *Geophys. Res. Lett.*, *28*, 291–294.
- Hansen, J. E., M. Sato, A. Lacis, R. Ruedy, I. Tegen, and E. Mathews (1998), Climate forcings in the Industrial era, *Proc. Natl. Acad. Sci. U. S. A.*, *95*, 12,753–12,758, doi:10.1073/pnas.95.22.12753.
- Hurt, G. C., S. Frolking, M. G. Fearon, B. Moore III, E. Shevliakova, S. Malyshev, S. W. Pacala, and R. A. Houghton (2006), The underpinnings of land-use history: Three centuries of global gridded land-use transitions, wood harvest activity, and resulting secondary lands, *Global Change Biol.*, *12*, 1208–1229.
- Jin, Y., C. B. Schaaf, F. Gao, X. Li, A. H. Strahler, X. Zeng, and R. E. Dickinson (2002), How does snow impact the albedo of vegetated land surfaces as analyzed with MODIS data?, *Geophys. Res. Lett.*, *29*(10), 1374, doi:10.1029/2001GL014132.
- Klein Goldewijk, K. (2001), Estimating global land use change over the past 3000 years: The Hyde database, *Global Biogeochem. Cycles*, *15*(2), 417–433.
- Klein Goldewijk, K., A. Beusen, G. van Drecht, and M. de Vos (2011), The HYDE 3.1 spatially explicit database of human-induced global land-use change over the past 12,000 years, *Global Ecol. Biogeogr.*, *20*, 73–86, doi:10.1111/j.1466-8238.2010.00587.x.
- Koster, R. D., and P. C. D. Milly (1997), The interplay between transpiration and runoff formulations in land surface schemes used with atmospheric models, *J. Clim.*, *10*, 1578–1591, doi:10.1175/1520-0442(1997)010<1578:TIBTAR>2.0.CO;2.
- Koster, R. D., et al. (2004), Regions of strong coupling between soil moisture and precipitation, *Science*, *305*, 1138–1140, doi:10.1126/science.1100217.
- Krinner, G., N. Viovy, N. de Noblet-Ducoudré, J. Ogée, J. Polcher, P. Friedlingstein, P. Ciais, S. Sitch, and I. C. Prentice (2005), A dynamic global vegetation model for studies of the coupled atmosphere-biosphere system, *Global Biogeochem. Cycles*, *19*, GB1015, doi:10.1029/2003GB002199.
- Lawrence, P. J., and T. N. Chase (2009), Climate impacts if making evapotranspiration in the Community Land Model (CLM3) consistent with the Simple Biosphere Model (SiB), *J. Hydrometeorol.*, *10*, 374–394.
- Lawrence, P. J., and T. N. Chase (2010), Investigating the climate impacts of global land cover change in the community climate system model, *Int. J. Climatol.*, *30*, 2066–2087.
- Loarie, S. R., D. B. Lobell, G. P. Asner, and C. B. Field (2011), Land-cover and surface water change drive large albedo increases in South America, *Earth Interact.*, *15*, Paper 7, doi:10.1175/2010EI342.1.
- Lyons, T. J., P. Schwerdtfeger, J. M. Hacker, I. J. Foster, R. C. G. Smith, and X. M. Huang (1993), Land atmosphere interaction in a semiarid region—The bunny fence experiment, *Bull. Am. Meteorol. Soc.*, *74*, 1327–1334, doi:10.1175/1520-0477(1993)074<1327:LIIASR>2.0.CO;2.
- Lyons, T. J., U. S. Nair, and I. J. Foster (2008), Clearing enhances dust devil formation, *J. Arid. Environ.*, *72*, 1918–1928, doi:10.1016/j.jaridenv.2008.05.009.
- Mahmood, R., S. A. Foster, T. Keeling, K. G. Hubbard, C. Carlson, and R. Leeper (2006), Impacts of irrigation on 20th century temperature in the northern Great Plains, *Global Planet. Change*, *54*, 1–18.
- Marshall, C. H., R. A. Pielke Sr., L. T. Steyaert, and D. A. Willard (2004), The impact of anthropogenic land-cover change on the Florida peninsula sea breezes and warm season sensible weather, *Mon. Weather Rev.*, *132*, 28–52, doi:10.1175/1520-0493(2004)132<0028:TIOALC>2.0.CO;2.
- Marti, O., et al. (2010), Key features of the IPSL ocean atmosphere model and its sensitivity to atmospheric resolution, *Clim. Dyn.*, *34*, 1–26, doi:10.1007/s00382-009-0640-6.
- Mathews, H. D., A. J. Weaver, M. Eby, and K. J. Meissner (2003), Radiative forcing of climate by historical land cover change, *Geophys. Res. Lett.*, *30*(2), 1055, doi:10.1029/2002GL016098.
- McGregor, J. L., and M. R. Dix (2008), An updated description of the Conformal-Cubic Atmospheric Model, in *High Resolution Simulation of the Atmosphere and Ocean*, edited by K. Hamilton and W. Ohfuchi, pp. 51–76, Springer, New York.
- Myhre, G., and A. Myhre (2003), Uncertainties in radiative forcing due to surface albedo changes caused by land-use changes, *J. Clim.*, *16*, 1511–1524.
- National Research Council (2005), *Radiative Forcing of Climate Change: Expanding the Concept and Addressing Uncertainties*, 224 pp., Natl. Acad. Press, Washington, D. C.
- Oleson, K. W., G. B. Bonan, S. Levis, and M. Vertenstein (2004), Effects of land use change on North American climate: Impact of surface datasets and model biogeophysics, *Clim. Dyn.*, *23*, 117–132, doi:10.1007/s00382-004-0426-9.
- Oleson, K. W., et al. (2008), Improvements to the Community Land Model and their impact on the hydrological cycle, *J. Geophys. Res.*, *113*, G01021, doi:10.1029/2007JG000563.
- Pielke, R. A., Sr., et al. (2011), Land use/land cover changes and climate: Modeling analysis and observational evidence, *WIREs Clim. Change*, *2*, 828–850, doi:10.1002/wcc.144.
- Pitman, A. J., et al. (2009), Uncertainties in climate responses to past land cover change: First results from the LUCID intercomparison study, *Geophys. Res. Lett.*, *36*, L14814, doi:10.1029/2009GL039076.
- Puma, M. J., and B. I. Cook (2010), Effects of irrigation on global climate during the 20th century, *J. Geophys. Res.*, *115*, D16120, doi:10.1029/2010JD014122.
- Raddatz, T., C. H. Reick, W. Knorr, J. Kattge, E. Roeckner, R. Schnur, K.-G. Schnitzler, P. Wetzel, and J. Jungclaus (2007), Will the tropical land biosphere dominate the climate-carbon cycle feedback during the twenty-first century?, *Clim. Dyn.*, *29*, 565–574.
- Ramankutty, N., and J. A. Foley (1999), Estimating historical changes in global land cover: Croplands from 1700 to 1992, *Global Biogeochem. Cycles*, *13*, 997–1027.

- Rayner, N. A., D. E. Parker, E. B. Horton, C. K. Folland, L. V. Alexander, D. P. Rowell, E. C. Kent, and A. Kaplan (2003), Global analyses of sea surface temperature, sea ice, and night marine air temperature since the late nineteenth century, *J. Geophys. Res.*, *108*(D14), 4407, doi:10.1029/2002JD002670.
- Roeckner, E., R. Brokopf, M. Esch, M. Giorgetta, S. Hagemann, L. Kornbluh, E. Manzini, U. Schlese, and U. Schulzweida (2006), Sensitivity of simulated climate to horizontal and vertical resolution in the ECHAM5 atmosphere model, *J. Clim.*, *19*, 3771–3791.
- Salas-Méllia, D., F. Chauvin, M. Déqué, H. Douville, J. F. Guérémy, P. Marquet, S. Planton, J. F. Royer, and S. Tyteca (2005), Description and validation of the CNRM-CM3 global coupled climate model, *Note 103*, Cent. du Groupe de Météorol. de Grande Echelle et Clim., Toulouse, France. [Available at http://www.cnrm.meteo.fr/scenario2004/paper_cm3.pdf]
- Seneviratne, S. I., R. D. Koster, Z. Guo, P. A. Dirmeyer, E. Kowalczyk, D. Lawrence, P. Liu, D. Mocko, K. W. Oleson, and D. Verseghy (2006), Soil moisture memory in AGCM simulations: Analysis of Global Land-Atmosphere Coupling Experiment (GLACE) data, *J. Hydrometeorol.*, *7*, 1090–1112.
- Seneviratne, S. I., T. Corti, E. L. Davin, M. Hirschi, E. B. Jaeger, I. Lehner, B. Orlowsky, and A. J. Teuling (2010), Investigating soil moisture-climate interactions in a changing climate: A review, *Earth Sci. Rev.*, *99*(3–4), 125–161, doi:10.1016/j.earscirev.2010.02.004.
- Snyder, P. K., C. Delire, and J. A. Foley (2004), Evaluating the influence of different vegetation biomes on the global climate, *Clim. Dyn.*, *23*(3–4), 279–302.
- Strengers, B. J., C. Müller, M. Schaeffer, R. J. Haarsma, C. Severijns, D. Gerten, S. Schaphoff, R. van den Houdt, and R. Oostenrijk (2010), Assessing 20th century climate-vegetation feedbacks of land-use change and natural vegetation dynamics in a fully coupled vegetation-climate model, *Int. J. Climatol.*, *30*(13), 2055–2065, doi:10.1002/joc.2132.
- Teuling, A. J., et al. (2010), Contrasting response of European forest and grassland energy exchange to heatwaves, *Nat. Geosci.*, *3*, 722–727, doi:10.1038/ngeo950.
- van den Hurk, B. J. J. M., P. Viterbo, A. C. M. Beljaars, and A. K. Betts (2000), Offline validation of the ERA40 surface scheme, *Tech. Memo.*, *295*, Eur. Cent. for Med.-Range Weather Forecasts, Reading, U. K.
- van der Molen M. K., B. J. J. M. van den Hurk, and W. Hazeleger (2011), A dampened land use change climate response towards the tropics, *Clim. Dyn.*, *37*, 2035–2043, doi:10.1007/s00382-011-1018-0.
- Voldoire, A. (2006), Quantifying the impact of future land-use changes against increases in GHG concentrations, *Geophys. Res. Lett.*, *33*, L04701, doi:10.1029/2005GL024354.